Characterizing Thermal Degradation in Semi-Crystalline Thermoplastic Composites

Mathew Wynn; Kuan-Ting Chen; Navid Zobeiry

OFFICIAL CONFERENCE PUBLICATION

Proceedings of the American Society for Composites - Thirty-Eighth Technical Conference (2023)
https://doi.org/10.12783/asc38/36599

ABSTRACT

Semi-crystalline thermoplastic composites, such as carbon fiber-reinforced polyetheretherketone (PEEK) and polyetherketoneketone (PEKK), are processed and consolidated while melted at high temperatures. During cool-down, polymer chains fold into lamellar structures at the nanoscale to form crystalline morphology. These lamellar structures radiate from a nucleus, creating spherulitic structures in bulk polymers, and transcrystallinity in fiber reinforced polymers. A certain amount of thermal degradation occurs when the thermoplastic matrix is melted, and the amount of degradation is a factor of several parameters such as melting temperature, time at melt, and whether the material is processed in an inert environment such as nitrogen. One form of degradation that occurs in the matrix is cross-linking and oxidation. In this case, the polymer chain breaks and new bonds form between chains or within the chain. Moreover, thermal degradation affects crystallization, the lamellar thickness and spacing, and overall degree of crystallinity. The spacing between lamellar structures can be measured through Small Angle X-ray Scattering (SAXS) at nanoscale, while the degree of crystallinity can be found using Wide Angle X-ray Scattering (WAXS).

To study thermal degradation, the effect of melting temperature, environmental condition, and reprocessing was investigated on samples of neat PEEK, as well as carbon-fiber PEKK prepreg. Additionally, these samples were thermally cycled multiple times, and repeats were performed for each condition. Degree of crystallinity, spacing, and lamellar thickness were measured using an x-ray scattering system. To study underlying physics and correlations, a probabilistic Machine Learning (ML) framework was used for regression. Using this approach, different thermal degradation mechanisms for neat resin and prepreg samples were demonstrated at the nanoscale. The differences were explained in terms of crystallinity and nucleation around fibers in prepreg. This framework provides a unique holistic understanding of crystal formation and degradation, which ultimately affects the reprocessability and end-part properties of semi-crystalline thermoplastic composites.

University of Washington, Materials Science & Engineering, 319 Roberts Hall, Box 352120, Seattle, WA 98195, U.S.A.

INTRODUCTION

Thermoplastic composites possess remarkable mechanical properties and are a candidate for replacing thermoset composite parts due to their reusability. These materials have a potential for reduced processing times and increased reprocessability, fueling a surge in utilization of thermoplastic composites across various industries. Within the aerospace sector, particular attention is given to implementing high-performance semi-crystalline thermoplastics like PEEK (Polyetheretherketone), PEKK (Polyetherketoneketone), and LM-PAEK (Low melt Polyaryletherketone). For instance, the International Space Station's mechanical arm features a PEEK composite, as do commercial aircraft brackets [1], [2]. To fabricate such components, thermoplastic composites are commonly consolidated and processed using techniques like automated fiber placement (AFP) followed by autoclave consolidation or compression molding. The resulting crystallinity of the end-part is greatly influenced by various parameters, including melt temperature history, dwell time, fiber volume fraction, and shear deformation history [3]–[5]. Without proper crystallization, these thermoplastics tend to exhibit amorphous properties, resulting in significantly reduced mechanical strength and limited chemical resistance.

Semi-crystalline thermoplastics can undergo degradation when exposed to prolonged periods at or above their melting temperature. This degradation process is exacerbated by higher melt temperatures and the presence of oxygen. The degraded material exhibits a higher glass transition temperature (T_g), reduced crystallinity, and lower melting temperature [6]. The degradation within the thermoplastic matrix affects the formation of crystals and alters the morphology. These changes typically arise from random molecular scission and subsequent cross-linking [7], which occur through bond formations within the polymer chain or between chains [8]. Consequently, these alterations hinder the recyclability and reworkability of the polymer while also modifying its mechanical and thermal properties.

Semi-crystalline thermoplastics like PEEK and PEKK form circular spherulites in the bulk polymer, and transcrystallinity when nucleating from a fiber. Examples of transcrystallinity and spherulites are provided in Figure 1. In Figure 1(a), transcrystallinity is observed on both fibers. Circular spherulites of varying sizes are visible in both Figure 1(a) and (b). When spherulites grow and impinge upon each other, growth stops at that interface and the spherulite becomes non-circular. The crystals shown in Figure 1 were stopped mid-growth, and the black region between them represents amorphous polymer that is yet to be crystallized. Typically, for PEEK, the entire surface is covered with crystals unless quenched.

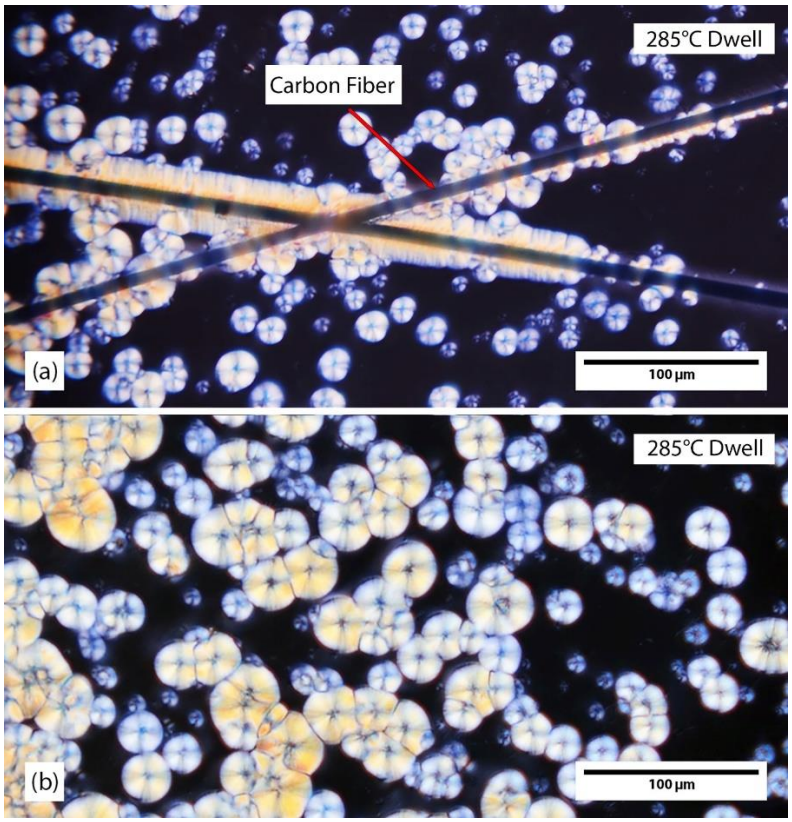

Figure 1. Examples of transcrystallinity and spherulites after a 285°C crystallizing dwell presented in a polarized light micrograph (a) shows a transcrystalline region growing from both fibers, Spherulites are observed in the surrounding material. (b) shows spherulites of varying sizes, with some impinging onto others and others isolated and still circular [9].

The crystalline features in semi-crystalline thermoplastics are comprised of lamella. An illustration of this lamellar structure is shown in Figure 2. Polymer chains fold back and forth to build up these lamellae, which are typically 5-20nm thick and surrounded by amorphous material. Small-angle x-ray scattering (SAXS) is a technique used to measure the thickness of these lamellar structures [10]. In SAXS, monochromatic x-rays are passed through the sample, which elastically scatters the x-rays and creates a two-dimensional scattering pattern. By integrating a slice of this pattern, a one-dimensional scattering curve is generated, providing information on nanoscale structures. SAXS is typically performed at scattering angles in the range of 0.1-10°.

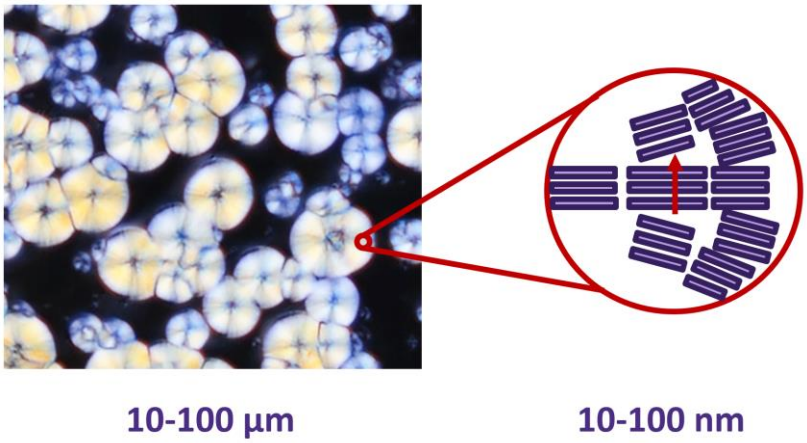

Figure 2. Lamellar stacking in a spherulite.

Another technique, wide-angle x-ray scattering (WAXS), can be used to gather information at the angstrom scale by performing scattering at wider angles, typically ranging from 10-55°. WAXS is used to identify Bragg peaks, and the area underneath the curves is related to the degree of crystallinity in the sample [11], [12]. The area underneath the curves will be affected by the carbon fiber reinforcement. With unidirectional reinforcement, the fiber angle can be changed with respect to the incident beam to minimize the effect on measuring crystallinity. However, given the complexities involved in data reduction and morphology analysis of semicrystalline composites via SAXS/WAXS methodologies, the role of advanced analytics and statistical techniques becomes more pronounced.

Machine Learning (ML) models have gained significant traction in recent years for various applications in composites. These include data reduction and correlation analysis of experimental results, real-time process simulation [13], [14], predicting shimming during assembly [15], characterizing damage [16]–[19], and detecting defects in automated fiber placement [20]. Among different ML approaches, probabilistic machine learning techniques like Gaussian Process Regression (GPR) have garnered considerable attention over traditional ML methods due to their effectiveness in training with small data [22], [23]. GPR, as a non-parametric regression approach [21], quantifies uncertainty in the model estimates rather than adopting a deterministic method to establish the underlying relationships in data. With the introduction of new data, the model can be retrained, thus improving the accuracy of predictions. Additionally, understanding the estimated model uncertainty can assist in subsequent data collection for targeted improvement of model accuracy.

In this study, we investigate the process-induced degradation of the crystalline structure in thermoplastics using a combined SAXS/WAXS experimental approach, complemented by GPR-based data analysis. We characterize the lamellar structure in PEEK neat film and PEKK-carbon fiber prepreg using x-ray scattering techniques following degradation induced by processing/reprocessing. We examine the effects of melt temperature, processing environment, and the number of reprocessing cycles on lamellar spacing, degree of crystallinity, and lamellar thickness. Changes in the lamellar structure are plotted using the response surface generated after training a GPR model to build a deeper understanding of the effects of degradation on crystallinity in semi-crystalline thermoplastic composites.

MATERIALS AND METHODS

Two types of materials were used: a PEKK-FC/AS4D prepreg from Solvay and a 25 µm thick PEEK film from Victrex (2000 series Aptiv). From these materials squares measuring approximately 6 by 6 mm were cut. One sample was directly placed onto a microscopic glass slide, while four other samples were positioned on a piece of Kapton film surrounding the first sample. The assembly, consisting of the glass slide, Kapton film, and samples, was then placed on a heating block inside a Linkam THMS600 hot stage, as depicted in Figure 3. The sample directly placed on the glass slide allowed for a representative view of all the samples and enabled in-situ polarizing light microscopic (PLM) observation of crystal growth [9], [21]. Unlike the sample placed directly on the glass, samples placed on the Kapton film could be removed and studied using x-ray scattering.

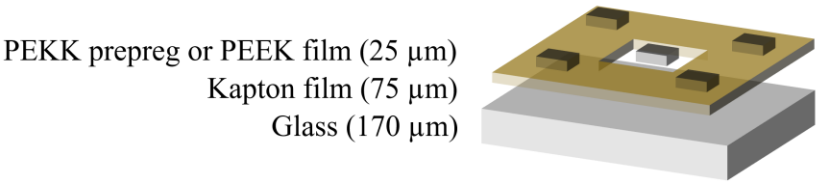

Figure 3. Sample configuration used in THMS600 hot stage [22].

Processing of samples using the THMS600 hot stage was performed under two different atmospheres: air (including oxygen), and nitrogen (i.e., inert). Initially, the samples were heated at a rate of 20 °C/min to 120 °C, and then held for 10 minutes to remove any moisture. Next, samples were heated to melt at a rate of 20 °C/min, and held for 10 minutes. Three different melt temperatures were utilized for each material. For the PEEK film, the standard melt temperature was set at 385 °C, an extreme high temperature at 420 °C, and a midpoint temperature at 400 °C. Notably, the temperature of 420 °C was chosen specifically to ensure the removal of prior crystallization history [23], [24]. As for the PEKK prepreg, which has a lower melting temperature, the temperatures employed were 410 °C, 392.5 °C, and 375 °C. Once the samples reached their respective melt temperatures, they were rapidly cooled at a rate of 140 °C/min to 285 °C for PEEK and 275 °C for PEKK, and then held at these temperatures for 10 minutes. The samples were then cooled down to 143 °C (T_g) at a rate of 65 °C/min. The cooling process was carried out as quickly as possible using the THMS600 hot stage to minimize crystallization during cooldown. A representation of the heating cycles for both is shown in Figure 4.

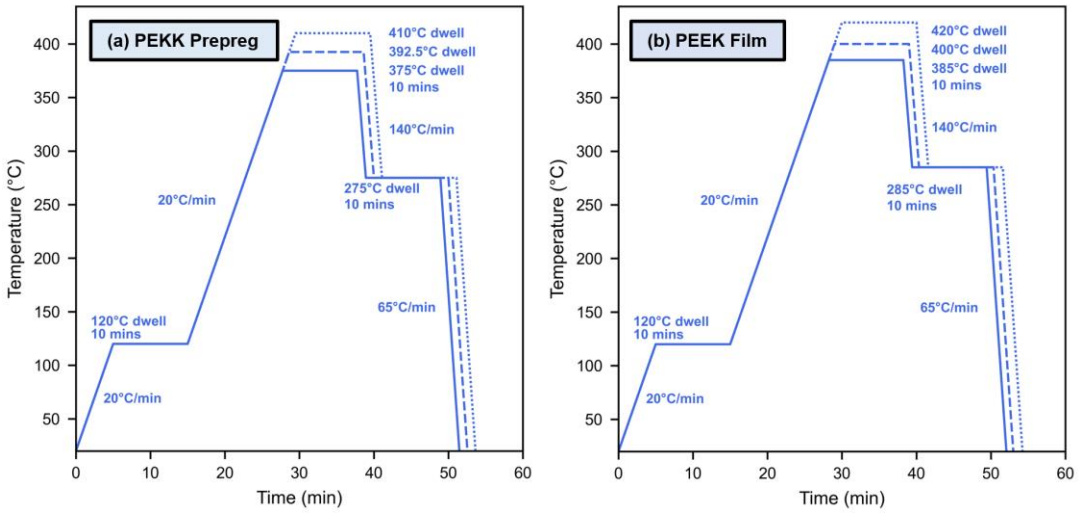

Figure 4. THMS600 heating cycles showing dwells and heating rates. (a) shows the heating cycle for PEKK prepreg (b) shows the heating cycle for PEEK film.

SAXS and WAXS were performed using a Xenocs Xeuss 3.0 System with a copper x-ray source with wavelength of 1.54Å and a Pilatus 300K detector. All measurements were performed under vacuum at an approximate pressure of 0.1 mbar and at room temperature. 2D scattering patterns were integrated using the Xeuss software to obtain I(q) data. The scattering vector **q** is defined as the difference between the scattered and incident wave vectors and is related to the scattering angle θ as follows:

$$\mathbf{q} = 4\pi \sin \frac{\theta}{\lambda} \tag{1}$$

where λ is the characteristic wavelength of copper at 1.54Å. SAXS was measured in the **q** range of 0.001 nm^{-1} to 3.0 nm^{-1}, and WAXS was measured in the **q** range 0.03 nm^{-1} to 6.8 nm^{-1}. Since the Xuess SAXS uses a slit collimator, SAXS data were Lorentz corrected.

Additionally, WAXS and SAXS were performed on an untreated piece of Victrex 2000G film, as an amorphous material. The SAXS curve was evaluated to ensure the absence of any peak, indicating no crystalline lamellar structure and likely no crystallinity. The WAXS curve of the untreated 2000G film was compared to other samples as an amorphous standard to calculate the degree of crystallinity.

RESULTS AND DISCUSSION

The collected WAXS data from the samples was compared to an amorphous standard. The area under the amorphous curve and the crystalline curve were determined by integration, and the degree of crystallinity was calculated as follows [25]:

$$Degree\ of\ Crystallinity = \frac{A_{crystal} - A_{amorphous}}{A_{crystal}}\ x\ 100\% \tag{2}$$

where $A_{crystal}$ is the area under the crystalline curve and $A_{amorphous}$ is the area under the amorphous curve.

The **q** value for the major peak observed in the SAXS curves was converted to 2θ using Equation (1, and then the long period (d) was calculated using Bragg's Law [26]:

$$d = \frac{n\lambda}{2\sin\theta} \tag{3}$$

where n is the diffraction order equal to one, λ is the characteristic wavelength of copper at 0.154nm, and θ is the angle of incidence. The lamellar thickness was obtained by multiplying the degree of crystallinity by the long period [27]. X-ray scattering data is provided in Table 1, showing that the lamellar thickness and degree of crystallinity decrease with an increase in melt temperature, cycle count, and processing in air instead of an inert nitrogen atmosphere. The long period is approximately the same across processing conditions. The observed lamellar thicknesses are consistent with previous results reported for PEEK, where thicknesses ranged from 2-6nm [28]–[30].

Table 1**.** PEEK Film X-ray Scattering Data

Melt Temperature (°C)	Environment	Cycles	Degree of Crystallinity (%)	Long period, *d* (nm)	Lamellar Thickness (nm)
385	Nitrogen	1	41.9	15.0	6.27
385	Nitrogen	3	37.6	14.9	5.59
385	Oxygen	1	37.3	14.7	5.49
385	Oxygen	1	36.2	14.6	5.29
385	Oxygen	3	39.0	14.6	5.70
420	Nitrogen	1	33.1	14.2	4.69
420	Nitrogen	3	30.8	15.5	4.77
420	Oxygen	3	30.1	14.1	4.23
400	Nitrogen	1	39.7	15.2	6.05
400	Nitrogen	3	36.2	14.1	5.09
400	Oxygen	1	39.5	14.6	5.78
400	Oxygen	3	38.5	14.2	5.45

Table 2 shows data collected for the PEKK prepreg samples. The long period measured in SAXS was approximately the same as the PEEK samples. The big difference is in degree of crystallinity, where crystallinity was significantly lower in the PEKK prepreg. The degree of crystallinity also changed much less and ranged from 23% to 26%, whereas the PEEK film ranged 30% to 41%. The result is the lamellar thickness is also lower than in the PEEK, and the range of change is smaller.

Table 2. PEKK Prepreg X-ray Scattering Data

Melt Temperature (°C)	Environment	Cycles	Degree of Crystallinity (%)	Long period (nm)	Lamellar Thickness (nm)
375	Nitrogen	1	23.18	14.29	3.31
375	Nitrogen	3	25.45	14.63	3.72
375	Oxygen	1	26.37	15.48	4.08
410	Nitrogen	1	25.98	14.86	3.86
410	Nitrogen	3	25.37	14.86	3.77
410	Oxygen	1	27.07	14.31	3.87
410	Oxygen	3	25.89	14.98	3.88
392.5	Nitrogen	1	26.39	14.29	3.77
392.5	Nitrogen	3	26.07	14.40	3.75
392.5	Oxygen	1	26.71	14.51	3.88
392.5	Oxygen	3	26.09	14.07	3.67

For GPR training, a covariance matrix (kernel) is selected, which is then utilized by GPR to make predictions and quantify uncertainty. During training, the posterior distribution is updated as more data is introduced, thereby reducing uncertainty and improving predictions [31].

Data was split into 80% training data and 20% validation data. For the kernel, the dot-product kernel was cubed and combined with the radial basis function (RBF) and white noise kernel:

$$\Sigma(x_i, x_j) = c * \left[\sigma_0^2 + x_i \bullet x_j\right]^3 + c * \exp\left(-\frac{d(x_i, x_j)^2}{2l^2}\right) + \sigma_e^2 I_n \quad (4)$$

where c is a constant, σ_0^2 is the inhomogeneity of the kernel, $d(x_i,x_j)$ is the Euclidean distance, l is the length scale of the kernel, σ_e^2 is the variance of noise, and I_n is the identity matrix. The length scale l was set to 1, and the default value of unity was used for both σ_0^2 and σ_e^2.

The x-ray scattering data for PEEK film and PEKK prepreg (Table 1 and Table 2) were fitted using trained GPR models. The resulting curves are displayed in Figure 5, showing a significant correlation between melt temperature and processing environment with the resulting lamellar thickness in the PEEK film. Generally, an increase in melt temperature results in lower lamellar thickness, whereas processing the sample in air leads to a further decrease in the lamellar thickness. Melt temperature has the most significant effect, followed by the processing environment (whether it is inert or in air). Cycle count had a minimal effect on lamellar thickness for both materials. There is a smaller effect in the PEKK prepreg, but the curve trends in the opposite direction with higher melt temperature and an oxygen environment leading to higher lamellar thickness.

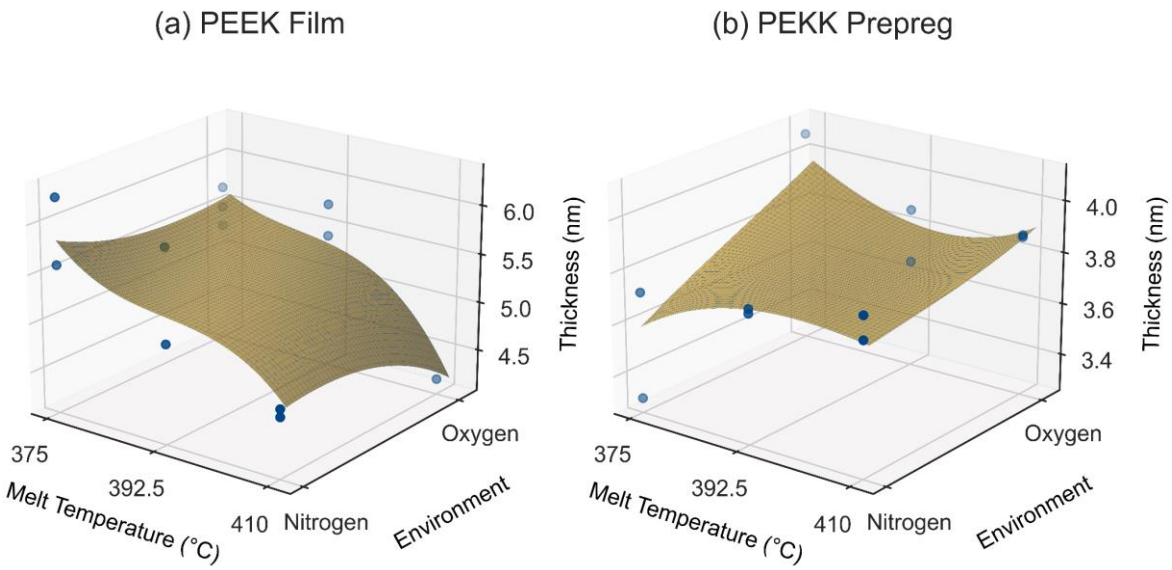

Figure 5. GPR surfaces fit to x-ray scattering data showing melt temperature, environment, and lamellar thickness (a) shows PEEK film (b) shows PEKK prepreg.

Similarly, curves were fitted with respect to the long period, and it was found that the long period had no correlation with the processing parameters discussed here. The degree of crystallinity displayed a similar relationship with process parameters as the lamellar thickness.

A significant effect was detected in the degree of crystallinity and lamellar thickness. The long period was found to be approximately the same between samples and materials. Strobl et al. discovered that the distance between lamellae, or the long period, is a function of the crystallization temperature, with increasing crystallizing temperatures allowing for more opportunity for new lamellae to form in between existing lamellae, decreasing the spacing [32]. In this study, the crystallizing temperature was kept constant at 285°C, so it follows that the spacing is approximately the same between thermal treatments. A portion of the polymer is likely cross-linked and can no longer participate in crystallization. These cross-linked polymers should also reduce the mobility of other polymers, slowing the crystal growth. This cross-linking and branching of the polymer chain increases the melt viscosity, which further slows the crystal growth [24]. Another mechanism of thermal degradation that does not involve cross-linking includes breakdown of the polymer chain into smaller molecular weight chains [33]. Smaller molecules will have less entanglement, which should increase mobility and thus chain folding and crystallization.

The PEKK prepreg yielded modest changes in degree of crystallinity and lamellar thickness with respect to changes in process parameters, especially when compared to the PEEK film. The addition of fibers may protect against the degradation effects seen in the neat PEEK. The fibers provide a large number of heterogeneous nucleation sites. This increased availability of nucleation may overcome thermal and oxidative degradation effects to some extent.

CONCLUSION

For PEEK, combined GPR and x-ray scattering showed decreasing degree of crystallinity and lamellar thickness, but no change in the long period, with increasing thermal exposure. Thermal treatment in air further decreased the degree of crystallinity and lamellar thickness. The PEKK prepreg had less degree of crystallinity and lower lamellar thickness compared with the PEEK film. In addition, the PEKK prepreg did not have a significant change in lamellar thickness or degree of crystallinity with respect to melt temperature, cycling, or environment. The fiber reinforcement in thermoplastic prepreg may limit degradation effects on crystallinity.

ACKNOWLEDGEMENTS

We would like to acknowledge financial support by the University of Washington and the State of Washington in the USA, as well as in-kind contributions of Victrex plc and Daher.

The authors acknowledge the use of facilities and instrumentation supported by the U.S. National Science Foundation through the Major Research Instrumentation (MRI) program (DMR-2116265) and the UW Molecular Engineering Materials Center (MEM-C), a Materials Research Science and Engineering Center (DMR-1719797).

REFERENCES

[1] J. Denault and M. Dumouchel, “Consolidation Process of PEEK/Carbon Composite for Aerospace Applications,” *Adv. Perform. Mater.*, vol. 5, pp. 83–96, 1998, doi: https://doi.org/10.1023/A:1008638105370.

[2] S. Green, F. J. Ferfecki, and U. Marburger, “Overmoulding of PEEK Compounds for Composites Aerospace Brackets,” *S.A.M.P.E. J.*, vol. 54, no. 3, pp. 22–29, 2018.

[3] J. Denault and T. Vu-Khanh, “Crystallization and Fiber/Matrix Interaction During the Molding of PEEK/Carbon Composites,” *Polym. Compos.*, vol. 13, no. 5, pp. 361–371, 1992.

[4] J. J. Tierney and J. W. Gillespie, “Crystallization kinetics behavior of PEEK based composites exposed to high heating and cooling rates,” *Compos. Part A Appl. Sci. Manuf.*, vol. 35, no. 5, pp. 547–558, 2004, doi: 10.1016/j.compositesa.2003.12.004.

[5] A. Lee, M. Wynn, L. Quigley, M. Salviato, and N. Zobeiry, “Effect of temperature history during additive manufacturing on crystalline morphology of PEEK,” *Adv. Ind. Manuf. Eng.*, vol. 4, p. 100085, May 2022, doi: 10.1016/j.aime.2022.100085.

[6] P. Tsotra, M. Toma, A. Pascual, F. Schadt, C. Brauner, and C. Dransfeld, “Thermo-Oxidative Degradation of Peek At High Temperatures,” 2018, no. June, pp. 24–28.

[7] M. Day, D. Sally, and D. M. Wiles, “Thermal degradation of poly(aryl-ether-ether-ketone): Experimental evaluation of crosslinking reactions,” *J. Appl. Polym. Sci.*, vol. 40, no. 910, pp. 1615–1625, Nov. 1990, doi: 10.1002/app.1990.070400917.

[8] A. Pascual, M. Toma, P. Tsotra, and M. C. Grob, “On the stability of PEEK for short processing cycles at high temperatures and oxygen-containing

atmosphere," *Polym. Degrad. Stab.*, vol. 165, pp. 161–169, 2019, doi: 10.1016/j.polymdegradstab.2019.04.025.

[9] M. Wynn and N. Zobeiry, "Investigating the Effect of Temperature History on Crystal Morphology of Thermoplastic Composites Using In Situ Polarized Light Microscopy and Probabilistic Machine Learning," *Polymers (Basel).*, vol. 15, no. 1, p. 18, Dec. 2022, doi: 10.3390/polym15010018.

[10] R. K. Verma, V. Velikov, R. G. Kander, H. Marand, B. Chu, and B. S. Hsiao, "SAXS studies of lamellar level morphological changes during crystallization and melting in PEEK," *Polymer (Guildf).*, vol. 37, no. 24, pp. 5357–5365, 1996, doi: 10.1016/S0032-3861(96)00387-4.

[11] A. A. Mehmet-Alkan and J. N. Hay, "The crystallinity of poly(ether ether ketone)," *Polymer (Guildf).*, vol. 33, no. 16, pp. 3527–3530, 1992, doi: 10.1016/0032-3861(92)91116-J.

[12] A. V. Fratini, E. M. Cross, R. B. Whitaker, and W. W. Adams, "Refinement of the structure of PEEK fibre in an orthorhombic unit cell," *Polymer (Guildf).*, vol. 27, no. 6, pp. 861–865, 1986, doi: 10.1016/0032-3861(86)90295-8.

[13] N. Zobeiry and K. D. Humfeld, "A physics-informed machine learning approach for solving heat transfer equation in advanced manufacturing and engineering applications," *Eng. Appl. Artif. Intell.*, vol. 101, p. 104232, May 2021, doi: 10.1016/j.engappai.2021.104232.

[14] M. Kim and N. Zobeiry, "Machine Learning for Reduced-order Modeling of Composites Processing," in *SAMPE Virtual Conference*, 2021, vol. accepted.

[15] K. Manohar, T. Hogan, J. Buttrick, A. G. Banerjee, J. N. Kutz, and S. L. Brunton, "Predicting shim gaps in aircraft assembly with machine learning and sparse sensing," *J. Manuf. Syst.*, vol. 48, pp. 87–95, Jul. 2018, doi: 10.1016/j.jmsy.2018.01.011.

[16] N. Zobeiry, J. Reiner, and R. Vaziri, "Theory-guided machine learning for damage characterization of composites," *Compos. Struct.*, vol. 246, p. 112407, Aug. 2020, doi: 10.1016/j.compstruct.2020.112407.

[17] J. Reiner, R. Vaziri, and N. Zobeiry, "Machine learning assisted characterisation and simulation of compressive damage in composite laminates," *Compos. Struct.*, vol. 273, p. 114290, Oct. 2021, doi: 10.1016/J.COMPSTRUCT.2021.114290.

[18] Y. Freed, M. Salviato, and N. Zobeiry, "Implementation of a probabilistic machine learning strategy for failure predictions of adhesively bonded joints using cohesive zone modeling," *Int. J. Adhes. Adhes.*, vol. 103226, 2022.

[19] Y. Freed, N. Zobeiry, and M. Salviato, "Development of aviation industry-oriented methodology for failure predictions of brittle bonded joints using probabilistic machine learning," *Compos. Struct.*, vol. 297, p. 115979, Oct. 2022, doi: 10.1016/J.COMPSTRUCT.2022.115979.

[20] C. Sacco, A. Baz Radwan, A. Anderson, R. Harik, and E. Gregory, "Machine learning in composites manufacturing: A case study of Automated Fiber Placement inspection," *Compos. Struct.*, vol. 250, p. 112514, Oct. 2020, doi: 10.1016/j.compstruct.2020.112514.

[21] M. Wynn and N. Zobeiry, "A Fast Method for Evaluating Effects of Process Parameters on Morphology of Semi-Crystalline Thermoplastic Composites," 2021.

[22] N. Zobeiry and M. Wynn, "INVESTIGATION OF DEGRADATION

EFFECTS ON CRYSTALLIZATION OF THERMOPLASTIC COMPOSITES," 2023, doi: 10.33599/nasampe/s.23.0216.

[23] S. Kumar, D. P. Anderson, and W. W. Adams, "Crystallization and morphology of poly(aryl-ether-ether-ketone)," *Polymer (Guildf).*, vol. 27, no. 3, pp. 329–336, 1986, doi: 10.1016/0032-3861(86)90145-X.

[24] A. Jonas and R. Legras, "Thermal stability and crystallization of poly(aryl ether ether ketone)," *Polymer (Guildf).*, vol. 32, no. 15, pp. 2691–2706, 1991, doi: 10.1016/0032-3861(91)90095-Z.

[25] G. Challa, P. H. Hermans, and A. Weidinger, "On the Determination of the Crystalline Fraction in Isotactic Polystyrene from X-Uay Diffraction," *Die Makromol. Chemie*, vol. 56, no. 1, pp. 169–178, 1962.

[26] A. Jonas, R. Legras, R. Scherrenberg, and H. Reynaers, "PEEK Oligomers: A Model for the Polymer Physical Behavior. 2. Structure and Thermal Behavior of Linear Monodisperse Oligomers," *Macromolecules*, vol. 26, no. 3, pp. 526–538, 1993, doi: 10.1021/ma00055a019.

[27] A. M. Jimenez, "Controlling Particle Structures in Polymers through Nanocomposite Processing," Columbia University, 2020.

[28] D. J. Blundell and B. N. Osborn, "The morphology of poly(aryl-ether-ether-ketone)," *Polymer (Guildf).*, vol. 24, no. 8, pp. 953–958, 1983, doi: 10.1016/0032-3861(83)90144-1.

[29] D. J. Blundell, "On the interpretation of multiple melting peaks in poly(ether ether ketone)," *Polymer (Guildf).*, vol. 28, no. 13, pp. 2248–2251, Dec. 1987, doi: 10.1016/0032-3861(87)90382-X.

[30] P. Cebe, S. Y. Chung, and S.-D. Hong, "Effect of thermal history on mechanical properties of polyetheretherketone below the glass transition temperature," *J. Appl. Polym. Sci.*, vol. 33, no. 2, pp. 487–503, Feb. 1987, doi: 10.1002/app.1987.070330217.

[31] J. Wang, "An Intuitive Tutorial to Gaussian Processes Regression," Sep. 2020, [Online]. Available: http://arxiv.org/abs/2009.10862.

[32] G. R. Strobl, M. J. Schneider, and I. G. Voigt-Martin, "Model of partial crystallization and melting derived from small-angle X-ray scattering and electron microscopic studies on low-density polyethylene," *J. Polym. Sci. Polym. Phys. Ed.*, vol. 18, no. 6, pp. 1361–1381, Jun. 1980, doi: 10.1002/pol.1980.180180615.

[33] C. L. Beyler and M. M. Hirschler, "Thermal Decomposition of Polymers," in *SFPE Handbook of Fire Protection Engineering 2*, 2002, pp. 111–131.